Effect of mixed plastic hardening on the cyclic contact between a sphere and a rigid flat

Effect of mixed plastic hardening on the cyclic contact between a sphere and a rigid flat

Yafei Mo[1], Rou Du[2*] and Xiaoming Liu[2]

[1] China Institute of Atomic Energy, Beijing 102413, P R China

[2] LNM, Institute of Mechanics, Chinese Academy of Sciences, Beijing 100190, P R China

First author's e-mail: myf_1979@126.com

[*]Corresponding author's e-mail: durou@imech.ac.cn

Third author's e-mail: xiaomingliu@imech.ac.cn

Abstract. This paper studies the effect of mixed plasticity mode (combined with isotropic and kinematic hardening law) on the cyclic contact between an elastic-plastic sphere and a rigid flat. Assuming power-law hardening with different levels of mixed plasticity for the sphere, we derived a semi-analytical expression of load versus interference during the first loading and unloading process. During cyclic loading, our results indicate that the isotropic plasticity model shows no variation of residual interference, while kinematic plasticity has the cyclic effect on the residual interference, and this effect is bigger for the material with a higher hardening exponent. In addition, we provided the semi-analytical expression for the evolution of residual interference, which is accurate for the strain hardening exponent from 0.1 to 0.5.

1. Introduction

Contacts between two bodies are widely found in engineering applications, such as bearings, mechanical seals, and joint structures. The prior studies on contact have been focused on the elastic sphere. For the small deformation (strain less than 1%), the well-known Hertz theory [1] can be used effectively. However, a large discrepancy would exist for the large deformation contact behavior of an elastic sphere. To partly overcome this limitation, Tatara [2] included forces on the opposite part of the sphere to accurately describe the contact with large deformation of the elastic sphere.

The subsequent studies extend from the elastic contact to the elastic-plastic contact. The prior studies have forced on analytical analysis to smooth the transition between elastic and plastic deformation. For example, Chang [3] used a linear interpolation method and Zhao et al. [4] used mathematical techniques. Apart from the analytical approach, the finite element method (FEM) offers an effective way to solve complex contact problems. Yan and Li [5] employed FEM to obtain the evolution of contact force, interference, and contact radius during cyclic oading conditions for elastic-perfectly plastic contact. Furthermore, Kogut and Etsion [6] derived the dimensionless expressions of contact load, contact area versus contact interference by using the FEM results.

The aforementioned researches have focused on elastic or elastic-perfectly plastic contacts, while the strain hardening effect of the deformable material has not been considered. Under this circumstance, Etsion et al. [7] studied an elastic-linear hardening sphere in contact with a rigid flat during the unloading process by analytical analysis. Later, this elastic-linear hardening contact was

extended to the multiple loading-unloading by Kadin et al. [8]. In their study, the elastic deformation after the first loading-unloading was appeared, which would be due to the assumed isotropic hardening. The other strain hardening type studied in the sphere contact is power-law hardening. For instance, the frictionless normal contact of two power-law hardening spheres was investigated by Mesarovic and Fleck to consider the effects of strain hardening rate, the relative size of the spheres and relative yield strength [9]. In addition, Olsson and Larsson [10] studied these two spheres' contact for the adhesive bodies. Their proposed analytical force-displacement relations were close to the FE results. In addition to the two spheres' contact, the power-law hardening has also been applied to the contact between a deformable sphere and a rigid flat. Zhao et al. [11] presented the relationship between contract load and contact interference for a large range of strain hardening exponent. It should be noted that those constitutive models used for the deformable materials have been assumed idealized isotropic hardening.

However, for the multiple loading-unloading conditions, we need to consider kinematic hardening in the elastic-plastic spherical contact. In the previous studies [12], the assumed pure isotropic hardening leads to the plastic shakedown phenomenon after the first loading-unloading cycle, which contradicts the real situation. Thus, Kadin et al. [8] indicated a hardening model that includes kinematic elements would be more realistic for the multiple loading-unloading contacts. In fact, the inelastic strain would be accumulated with the asymmetrical stress-controlled cycles. This phenomenon is called ratcheting. The first kinematic hardening model to describe ratcheting is the Armstrong-Frederick (AF) model [13]. However, this model overestimates the ratcheting strain. Due to this fact, the type of Chaboche model has been developed [14]. For example, by using the Chaboche model, Pual et al. [15] predicted the ratcheting behavior of SA333 C-Mn steel under different loading conditions. In the literature, all those kinematic hardening models have been focused on no-contact deformation behavior. To the authors' knowledge, no work has been used those kinematic hardening models in the spheric contact mechanics to describe the spheric multiple loading-unloading.

In this study, we first carry out FE solutions for a power-law hardening elastic-plastic sphere with different strain hardening exponents. In addition, different strain hardening modes are employed. Then, the analytical relation between contact load and the contact interferences during cyclic loading contacts are presented based on the FE results.

2. Definition of contact model

The contact condition of a deformable sphere with a rigid flat is presented in Figure 1. The dash lines and solid lines represent the profile of the deformable sphere before and after contact, respectively. In Figure 1(a), δ is interference, r is contact radius and P is contact force during loading. The unloading parameters are presented in Figure 1(b), where $\delta_{\max}$ is maximum interference and δ_{res} residual interference.

Under the frictionless contact condition, the critical interference can be calculated by [3]:

$$\delta_c = (\frac{\pi KH}{2E})^2 R \tag{1}$$

where H is hardness, K is a coefficient related to the Poisson ratio, and E is the elastic modulus. The detailed expressions of H, K, and E can be found in [6].

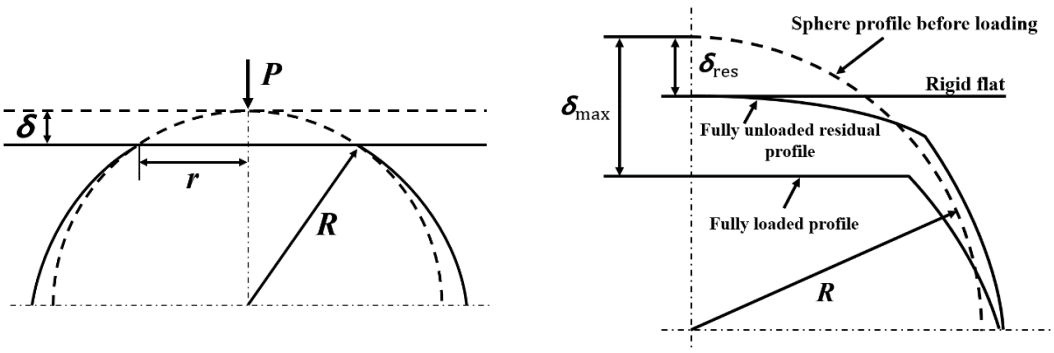

(a) (b)

Figure 1. The demonstration of contact geometry between a deformable sphere and a rigid flat in: (a) the loading condition and (b) the unloading condition.

3. Finite element model

3.1. Material constitutive model

In this study, we assume the deformable sphere to be elastic-plastic; and the plastic behavior follows:

$$f = \sqrt{3J_2(\boldsymbol{\sigma} - m\boldsymbol{\alpha})} - \sigma_0 - (1-m)R = 0 \tag{2}$$

where $\boldsymbol{\sigma}$ is the stress tensor, $\boldsymbol{\alpha}$ is the back stress tensor, $J_2()$ is the second invariant of a tensor, σ_0 is the initial yielding stress, and *R* donates the isotropic hardening with respect to the accumulated plastic strain. The parameter *m* represents the strain hardening mode: $m = 0$ and $m = 1$ represent isotropic hardening and kinematic hardening, respectively, and $0 < m < 1$ represents combined hardening.The evolution of $\boldsymbol{\alpha}$ is represented by the classic Chaboche model [14]. The strain hardening is considered under a power hardening law. Under the uniaxial condition, the relation between the stress σ and the strain ε is given by:

$$\varepsilon = \begin{cases} \sigma / E & \sigma \le \sigma_0 \\ (\sigma_0 / E)(\sigma / \sigma_0)^{1/n} & \sigma > \sigma_0 \end{cases} \tag{3}$$

where *n* gives the strain hardening exponent.

3.2. Finite element model

An axisymmetric FE model was built up with the commercial software ABAQUS 6.14. As shown in Figure 2, only a quarter of the sphere was used due to the symmetric feature. In the model, the quarter sphere was divided into two zones with different mesh sizes: fine mesh in the zone I (inside 0.1R) and coarse mesh in the zone II (outside of 0.1R). The typical mesh size in the zone I was $0.028\, r_c$ ($r_c = (R\delta_c)^{1/2}$), and the mesh size was gradually increased in the Zone II. A rigid flat was used, and the contact was set to be frictionless. After a convergence study, we found out that the current model, consisting of about 27000 four-node axisymmetric elements, could provide results with sufficient accuracy. Also, we have used Hertz solution to verify the accuracy of this model.

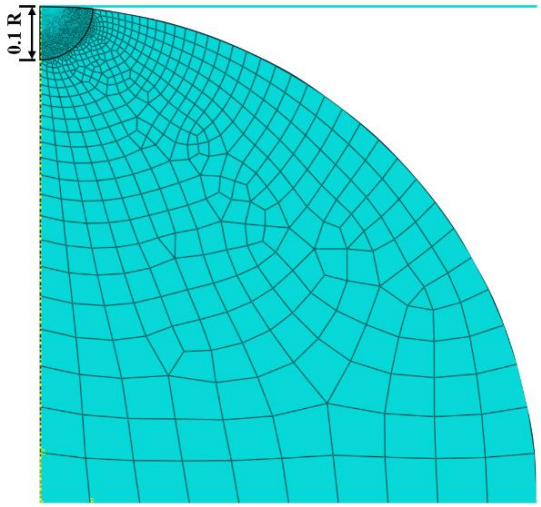

Figure 2. The finite element model

4. Results and discussions

4.1. Plastic contact effect on the loading process

In this section, the loading behavior is analyzed by considering the effect of strain hardening exponent n and strain hardening mode m. First, the contact load P / P_c and the contact interferences δ / δ_c are calculated under isotropic hardening and kinematic hardening with strain hardening exponent n equal to 0.1, 0.3 and 0.5, respectively. The corresponding results are shown in Figure 3. As expected, the contact load increases with the strain hardening exponent for the fixed strain hardening mode. While for the different strain hardening modes, the discrepancy between isotropic hardening and kinematic hardening is minimal at n = 0.1. Furthermore, this difference increases with increasing hardening exponent, as shown in the amplification part of Figure 3.

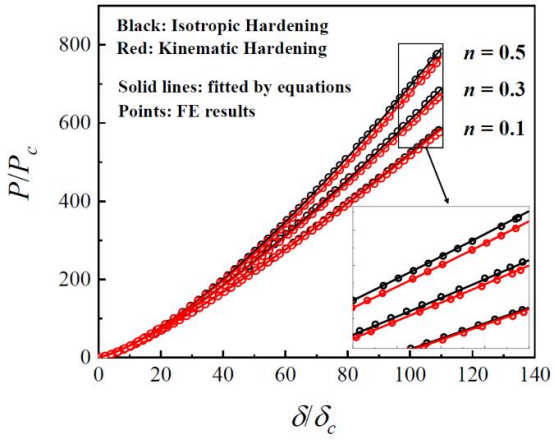

Figure 3. Dimensionless contact load (P / P_c) against dimensionless interference δ / δ_c in contact loading condition under different strain hardening modes

Then, in order to describe the curves analytically under different strain hardening exponents and modes, we express the following relations:

$$\frac{P}{P_c} = b_1 \left(\frac{\delta}{\delta_c}\right)^{b_2} \tag{4}$$

where b_1 and b_2 are two coefficients and can be related to hardening exponent n in the range of $\delta / \delta_c \le 110$. To consider the influence of hardening mode, the parameter m is introduced in the expression of b_2. Fitted with the FE results by using the least square method, these coefficients are expressed as:

$$b_1 = f_1(n) = -0.9975n + 1.8317 \tag{5}$$

$$b_2 = f_2(n,m) = 0.2978n - 0.0117mn + 1.2095 \tag{6}$$

As shown in Figure 3, the FE based Eqs. (4)-(6) can characterize the first loading behavior in the range of $\delta / \delta_c \le 110$ under different hardening modes.

4.2. Plastic contact effect on the unloading process

The unloading behavior is another important aspect during the cyclic loading-unloading processes. The FE simulations of the unloading process with different strain hardening exponents n and strain hardening modes m have been performed. In those simulations, the relations of the contact load P / P_c and contact interference δ / δ_c have been calculated, and the results of $\delta_{\max} / \delta_c$ = 110 and 60 are shown in Figure 4. To present the analytical expression of those relations clearly, we define $\delta^* = \delta / \delta_c$, $\delta^*_{\max} = \delta_{\max} / \delta_c$, $P^* = P / P_c$ and $P^*_{\max} = P_{\max} / P_c$. Based on the previous works [7, 11], we propose the following new expression:

$$P^* = P^*_{\max} \left(\frac{\delta^* - \delta^*_{res}}{\delta^*_{\max} - \delta^*_{res}} \right)^{h_p} \tag{7}$$

the exponent of the above equation can be written as:

$$h_p = 1.5(\delta^*_{\max})^{e_p} \exp(0.6214mn) \tag{8}$$

where the item $\exp(0.6214mn)$ includes the influence of hardening mode, e_p is a function of n with the following expression:

$$e_p = f_e(n) = -0.0556n^2 + 0.058n - 0.0454 \tag{9}$$

Figure 4 presents a comparison between the analytical results by Eqs. (7)-(9) and the corresponding FE results. It shows that these dimensionless equations can describe the unloading behavior accurately.

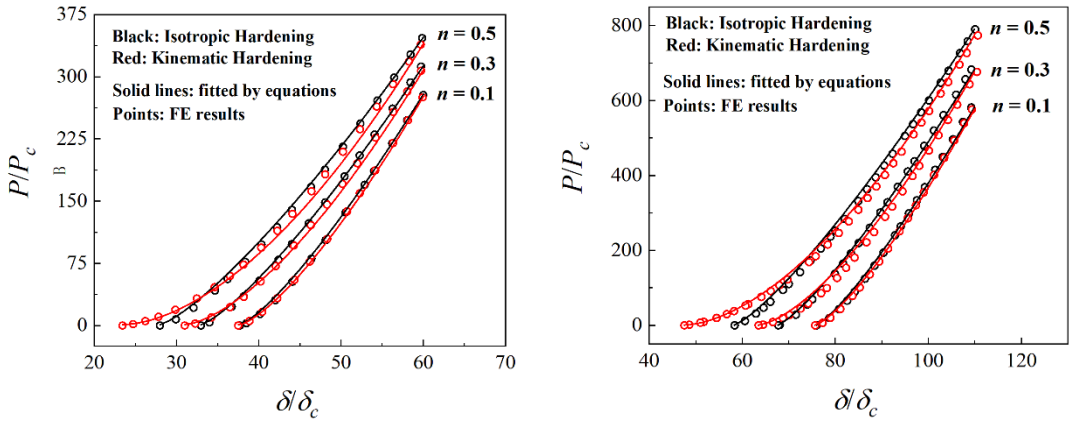

Figure 4. Dimensionless contact load P / P_c with the dimensionless interference δ / δ_c during the unloading process: (a) $\delta / \delta_c = 60$; (b) $\delta / \delta_c = 110$

The unloading process can also be featured by the residual interference δ_{res} and the maximal interference $\delta_{\max}$. However, only isotropic hardening has been considered in a previous study [11]. As

shown in Figure 5 (a), the relation between δ_{res} and $\delta_{\max}$ is also related to the strain hardening mode. As a result, we further include the influence of strain hardening mode on this relation:

$$\frac{\delta_{res}}{\delta_{\max}} = (1 - \frac{1}{(\delta_{\max} / \delta_c)^d})^2 (\delta_{\max} / 5\delta_c)^{(-0.1263 m^2 n)} \tag{10}$$

where m is introduced by the term $(\delta_{\max} / 5\delta_c)^{(-0.1263 m^2 n)}$ to represent this influence. The above equation returns to the isotropic hardening mode when $m = 0$, which is identical to the expression in the previous work [11]. Also, d is the function of n and can be expressed as:

$$d = g(n) = -0.0533 n^2 - 0.2383 n + 0.4157 \tag{11}$$

As shown in Figure 5(a), the analytical results can accurately describe the FE results in the unloading profile for two hardening modes. For a fixed hardening mode, $\delta_{\text{res}} / \delta_{\max}$ increases with increasing $\delta_{\max} / \delta_c$ and decreasing n. On the other hand, the difference of $\delta_{\text{res}} / \delta_{\max}$ between two hardening is obvious, especially under the condition of $n = 0.5$ and $\delta_{\max} / \delta_c = 110$. Thus, we check the description capacity of Eqs. (10) and (11) for different values of m under this condition. Figure 5(b) shows a good agreement between the analytical and the finite element results.

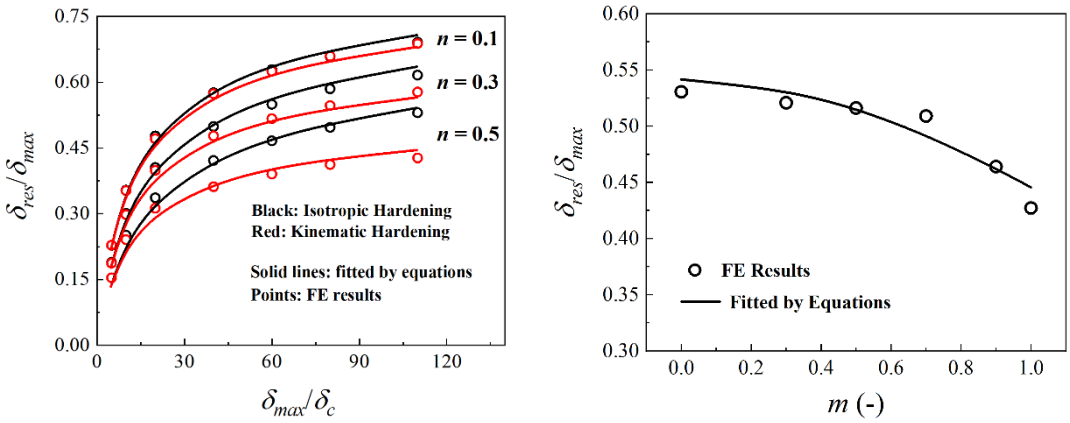

(a) (b)

Figure 5. Dimensionless residual interference ($\delta_{\text{res}} / \delta_{\max}$) to (a) dimensionless maximum interference ($\delta_{\max} / \delta_c$) and (b) hardening mode (m) at n=0.5 and $\delta_{\max} / \delta_c = 110$

4.3. Multiple loading-unloading processes

We studied the plastic effect on multiple cycles, in which 25 loading-unloading cycles are performed under different strain hardening exponents and modes with the initial maximum dimensionless interference around 110. From the numerical simulations, we obtain the relationships between contact load P / P_c and contact interference δ / δ_c. As shown in Figure 6(a, b, c) for the isotropic hardening mode, the shakedown phenomena are observed after the first loading-unloading cycle under all strain hardening exponents. However, for the kinematic hardening mode (Figure 6(d, e, f)), the maximum interference increases continuously with the cyclic number, and its growth from one cycle to another cycle increases with increasing n.

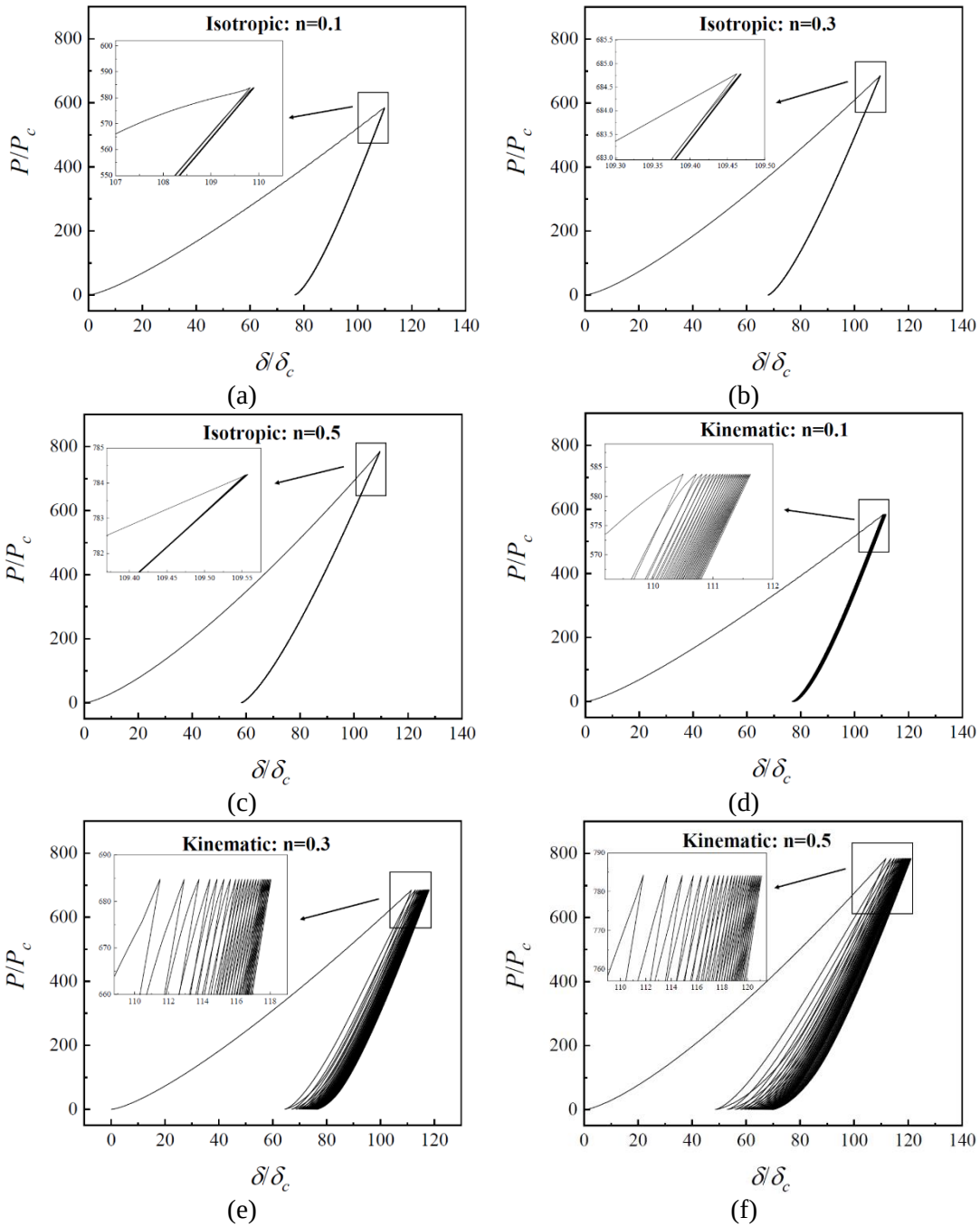

Figure 6. Dimensionless contact load (P / P_c) against dimensionless interference δ / δ_c during 25 loading-unloading cycles for: (a, b, c) isotropic hardening and (d, e, f) kinematic hardening at different strain hardening exponent

Those multiple cyclic behaviors of different hardening modes are related to the involved plastic strain. Under the multiple loading-unloading, the plastic strain occurs only near the contact area, as shown in Figure 7(a). Thus, the following discussion is mainly focused on this area. Figure 7(b) and (c) display the magnification of equivalent plastic strain distribution after 25 multiple cycles for hardening exponent $n = 0.5$ under isotropic hardening and kinematic hardening, respectively. It can be seen that the plastic deformed location is similar for both hardening modes. However, the value of equivalent plastic strain exhibits a large difference: the maximum value for kinematic hardening is 5.5×10^{-2}

while for isotropic hardening is only 5.5×10^{-3}. We also output the evolution of maximum equivalent plastic strain with the cyclic number for both hardening modes. As shown in Figure 7(d), for isotropic hardening, the maximum equivalent plastic strain remains constant after the first loading-unloading cycle. This means no plastic deformation happens for the following cycles. In the meantime, the maximum equivalent plastic strain under kinematic hardening continues to increase with the cyclic number. This is due to the used kinematic hardening rule. In the multiple loading-unloading conditions, asymmetric stress-controlled cycles exist in the deformed region. Under those cycles, the classic Chaboche model, used as our kinematic hardening rule, can lead to continuous growing ratcheting strain [16, 17]. As a result, continuous plastic deformation occurs under this kinematic strain hardening model. In conclusion, the plastic deformation continues with cyclic loading-unloading under the kinematic hardening mode and stops after the first cycle under the isotropic hardening mode.

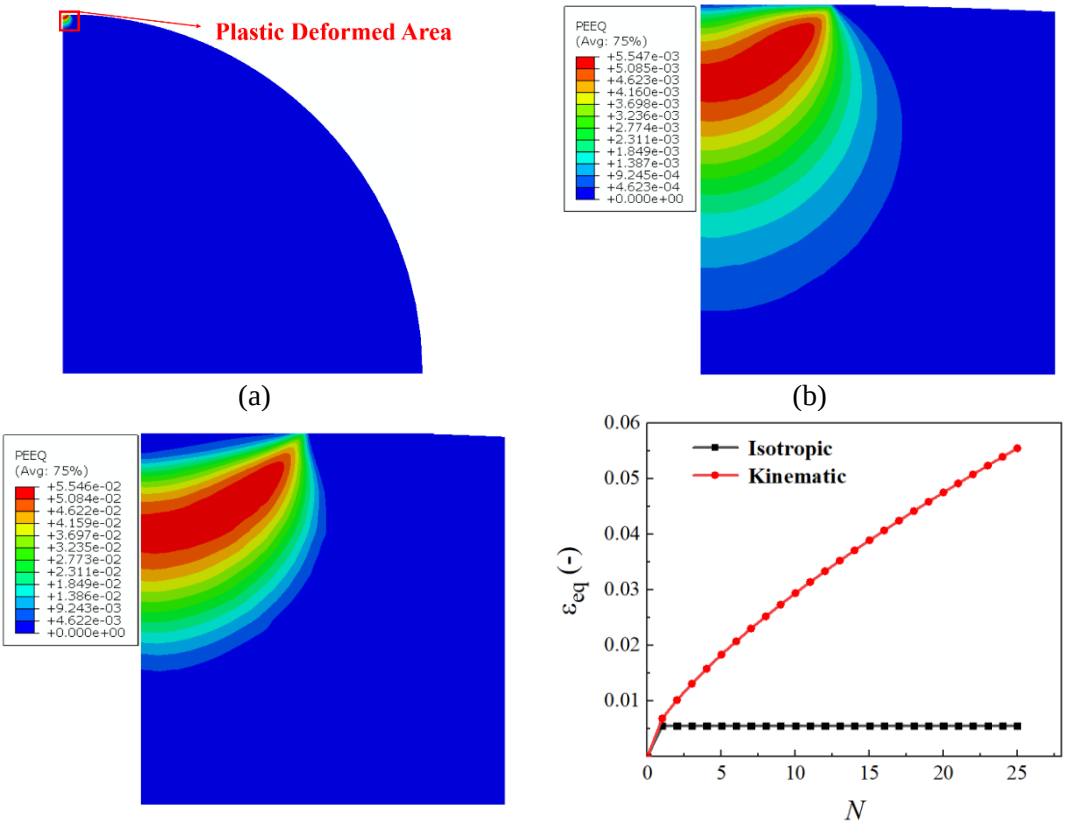

Figure 7. (a)Illustration of equivalent plastic strain distribution after 25 cycles; magnification of equivalent plastic strain distribution for (b) isotropic hardening mode and (c) kinematic hardening mode; (d) evolution of maximum equivalent plastic strain against the cyclic number for both hardening modes

As the shakedown phenomena are observed after the first loading-unloading cycle for the isotropic hardening, the analytical expression for the evolution of maximum interference with the cycles is only discussed for the kinematic hardening mode. To predict the evolution of maximum interference, the dimensionless maximum interference $\delta_{\max} / \delta^1_{\max}$ can be expressed as:

$$\frac{\delta_{\max}}{\delta^1_{\max}} = N^d \tag{12}$$

where $\delta^1_{\max}$ is the maximum interference of the first cycle, d is as the function of n:

$$d = f_d(n) = -0.1058n^2 + 0.1185n - 0.0078 \quad (13)$$

As shown in Figure 8, Eq. (12) can be used to characterize the multiple loading-unloading cycles under pure kinematic hardening.

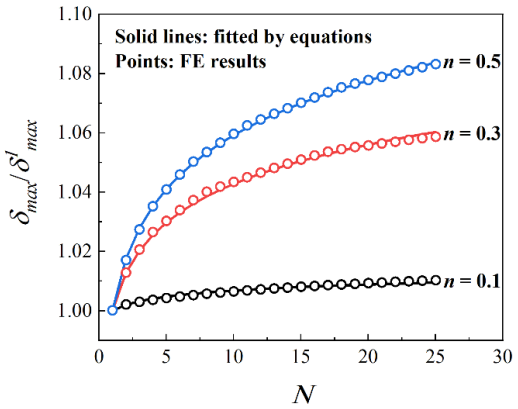

Figure 8. Ratio of subsequent maximum interference to first maximum interference versus cycle number for repeated loading

5. Conclusion

The influence of hardening mode (m) and hardening exponent (n) on the frictionless contact behavior were studied. The following conclusions are summarized:

1) The contact load in the first loading increases with the increasing n and decreasing m.
2) The residual interference after first complete unloading correlates to the maximum loading interference.
3) For the multiple loading-unloading processes, the interference continues to grow under the kinematic hardening, while the shakedown phenomenon is observed for the isotropic hardening after the first cycle.
4) Under the kinematic hardening, the maximum interference growth in each cycle increases with increasing n.

It should be noted that phenomenological constitutive models are used in our study. In the future work, we could consider the influence of microstructure and develop a physics-informed model to study the contact behavior.

Acknowledgements

This work was supported by the National Natural Science Foundation of China (No. 11772334, 12022210, 12032001).

References

[1] Johnson, K.L. (1985) Contact mechanics. MA: Cambridge university press, Cambridge.
[2] Tatara, Y. (1991) On Compression of Rubber Elastic Sphere Over a Large Range of Displacements-Part 1: Theoretical Study. J. Eng. Mater. Technol., 113(3): 285-291.
[3] Chang, W.R., Etsion, I., Bogy, D.B. (1987) An Elastic-Plastic Model for the Contact of Rough Surfaces. J. Tribology, 109(2): 257-263.
[4] Zhao, Y., Maietta, D.M., Chang L. (1999) An Asperity Microcontact Model Incorporating the Transition From Elastic Deformation to Fully Plastic Flow. J. Tribology, 122(1): 86-93.
[5] Yan, S.L., Li, L.Y. (2003) Finite element analysis of cyclic indentation of an elastic-perfectly plastic half-space by a rigid sphere. Proceedings of the Institution of Mechanical Engineers, Part C: Journal of Mechanical Engineering Science, 217(5): 505-514.
[6] Kogut, L. and Etsion, I. (2002) Elastic-Plastic Contact Analysis of a Sphere and a Rigid Flat. J. Appl. Mech., 69(5): 657-662.

[7] Etsion, I., Kligerman, Y., Kadin, Y. (2005) Unloading of an elastic–plastic loaded spherical contact. Int. J. Solids Struct., 42(13): 3716-3729.
[8] Kadin, Y., Kligerman, Y. Etsion, I. (2006) Multiple loading–unloading of an elastic–plastic spherical contact. Int. J. Solids Struct., 43(22-23): 7119-7127.
[9] Mesarovic, S.D., Fleck, N.A. (2000) Frictionless indentation of dissimilar elastic–plastic spheres. Int. J. Solids Struct., 37(46): 7071-7091.
[10] Olsson, E., Larsson, P.L. (2013) On force–displacement relations at contact between elastic–plastic adhesive bodies. J. Mech. Phys. Solids, 61(5): 1185-1201.
[11] Zhao, J.H., Nagao, S., Zhang, Z.L. (2012) Loading and unloading of a spherical contact: From elastic to elastic–perfectly plastic materials. Int. J. Mech. Sci., 56(1): 70-76.
[12] Song, Z., Komvopoulos, K. (2014) An elastic–plastic analysis of spherical indentation: Constitutive equations for single-indentation unloading and development of plasticity due to repeated indentation. Mech. Mater ., 76: 93-101.
[13] Armstrong, P.J., Frederick, C.O. (1966) A mathematical representation of the multiaxial Bauschinger effect. CEGB Report RD/B/N731, Berkeley Nuclear Laboratories.
[14] Chaboche, J.L. (1989) Constitutive equations for cyclic plasticity and cyclic viscoplasticity. Int. J. Plast., 5(3): 247-302.
[15] Paul, S.K., et al. (2010) Simulation of cyclic plastic deformation response in SA333 C–Mn steel by a kinematic hardening model. Compu. Mater. Sci., 48(3): 662-671.
[16] Kalnins, A., Rudolph, J., Willuweit, A. (2015) Using the Nonlinear Kinematic Hardening Material Model of Chaboche for Elastic–Plastic Ratcheting Analysis. J. Press. Vessel. Technol.,137(3).
[17] Moslemi, N., et al. (2020) Uniaxial and biaxial ratcheting behavior of pressurized AISI 316L pipe under cyclic loading: Experiment and simulation. Int. J. Mech. Sci., 179: 105693.